Phonon scattering mechanisms in suspended nanostructures from 4 to 40 K

W. Fon,[1] K. C. Schwab,[2] J. M. Worlock,[1,3] and M. L. Roukes[1]
[1]*Condensed Matter Physics, California Institute of Technology, mail code 114-36, Pasadena, California 91125*
[2]*Laboratory for Physical Sciences, University of Maryland, College Park, Maryland 20740*
[3]*Department of Physics, University of Utah, Salt Lake City, Utah 84112*
(Received 12 February 2002; published 9 July 2002)

We have developed specially designed semiconductor devices for the measurement of thermal conductance in suspended nanostructures. By means of a novel subtractive comparison, we are able to deduce the phonon thermal conductance of individual nanoscale beams of different geometry and dopant profiles. The separate roles of important phonon scattering mechanisms are analyzed and a quantitative estimation of their respective scattering rates is obtained using the Callaway model. Diffuse surface scattering proves to be particularly important in the temperature range from 4 to 40 K. The rates of other scattering mechanisms, arising from phonon-phonon, phonon-electron, and phonon-point defect interactions, also appear to be significantly higher in nanostructures than in bulk samples.

DOI: 10.1103/PhysRevB.66.045302 PACS number(s): 63.22.+m, 66.70.+f, 81.07.−b

I. INTRODUCTION

Phonon transport and scattering mechanisms in *bulk* crystalline GaAs and other semiconductors are well characterized by measurement of thermal conductance and other well-established experimental techniques.[1–4] However, there is not yet a systematic experimental method for studying phonon thermal transport within nanoscale semiconductor structures. As described more fully below, past investigations have suffered from the fact that the electrical transducers and their connections, necessary for thermal conductance measurements, often have provided a parasitic thermal path that overwhelms the contribution from phonons. In this paper, we describe measurements of the thermal conductance in specially designed nanostructures which enable the phonon thermal conductance of undoped dielectric (insulating) semiconductor beams and doped (electrically conducting) beams to be separately deduced. The conductance data from the dielectric beams at low temperatures (<10 K) enable investigation of the effect of diffuse surface scattering of phonons. Thermal conductance data from the dielectric beams at higher temperatures (20–40 K), at which umklapp processes turn on, show the effects of phonon-phonon scattering. Comparison of the conductance of undoped and doped beams at low temperatures provides information about phonon-electron scattering. At higher temperatures, this same comparison yields information regarding phonon-defect scattering. Application of the Callaway analysis[2] enables the rates of each of these separate scattering mechanisms to be estimated quantitatively.

Early work on the thermal conductance of suspended submicron diameter beams showed that thermal transport due to electrons dominates that of phonons from 0.5 to 4 K.[5] This, however, may have been the result of the limited amount of heat transferred to the lattice from the heat source, given the relatively weak electron-phonon coupling present at low temperatures.[6] Later work by Tighe *et al.*[7] on suspended structures with separate heaters and thermometers reduced the obfuscating thermal conductance arising from electron diffusion and thereby provided a more direct measurement of phonon transport. This work showed that phonons can indeed provide the major pathway for heat transport above 2 K in semiconductor nanostructures.

In macroscopic samples below 40 K, a regime where umklapp phonon-phonon scattering is suppressed, it is well known that phonons can propagate ballistically for a long distance, of the order of centimeters, within a bulk crystal.[8] In this regime, scattering predominantly occurs at the surfaces of the specimen; in clean, highly polished dielectric crystals of macroscopic size below 1 K more than 99% of the incident phonons can specularly reflect from surfaces.[9] Thus, in such a crystal sample, thermal energy is transported efficiently, and the influence of phonon scattering is minimal. On the other hand, for nanostructures of microscopic size, experiments to date seem to indicate that phonon scattering *always* plays an important role in thermal transport, even at very low temperatures. The work of Tighe *et al.* showed that diffuse surface scattering of phonons in suspended nanostructures is dominant from 1 to 10 K. In their study, phonons were specularly reflected at the surface only about twice on average, before being diffusely scattered.

The effect of dimensionality can also be very significant on the transport of phonons in nanostructures. Schwab *et al.* demonstrated that for a short, narrow constriction (<100 nm) at very low temperature (<0.3 K), the phonon transport becomes one dimensional and the universal thermal conductance was observed.[11] In our experiment, on the other hand, the phonon wavelength (~ 10 nm at 4 K) remains small compared to the cross section of the beam. Therefore, the phonon transport in our experiment is best analyzed by a three-dimensional model.

II. SAMPLES AND EXPERIMENTAL METHOD

Our suspended devices are fabricated from GaAs/AlGaAs heterostructures grown by molecular beam epitaxy. The $\approx 1-\mu$m-thick AlGaAs sacrificial layer below the device is removed during the fabrication to suspend specific GaAs features with nanometer-scale dimensions. The 150-nm-thick single-crystalline GaAs layer is nonuniformly doped. The

lower 100 nm GaAs layer is intrinsic (undoped) and is patterned into a hexagonal reservoir and suspended, thermally conducting beams that connect the device to the heat sink (substrate). The topmost 50 nm layer is degenerately Si-doped $n+$ GaAs ($N_D=5\times10^{18}$ cm^{-3}). From it are patterned the electrical transducers and their electrical connections; these consist of two resistive meanders atop the reservoir and conducting leads that run from them atop the beams to provide connection to the external electrical contacts. The meanders constitute electrical transducers that act as heat source and temperature sensor. The technique and procedure of fabrication are similar to those described by Tighe *et al.*[7]

The unique aspect of the experiments reported here involves comparative measurements on two types of suspended devices. One set of such devices is depicted in Fig. 1. Figure 1(a) shows a four-beam device, comprising a central hexagonal reservoir that is connected to the heat sink by four of what we term "*doped beams*." Each is 6 μm long, 250 nm wide, and 150 nm thick. These are not uniformly doped; only the topmost 50 nm of them is a $n+$ conducting layer, as shown in Fig. 1(c). Evident in Fig. 1(a) also are the meanders of $n+$ material on the top of the hexagonal reservoir. These meandering resistors act as heater and thermometer. The six-beam device [Fig. 1(b)] has two additional *undoped beams* [Fig. 1(c)] from which the $n+$ conducting layer is removed. In these thermal conduction is purely phononic and does not suffer from interactions with electrons or donors. All devices are constructed to the same dimensions, to within the few percent dimensional tolerances achievable by our electron-beam-lithography-based surface nanomachining process. The four- and six-beam device pairs are cofabricated in close proximity on the same chips and are therefore subjected to identical pattern-writing and -etching processes.

Measurement of devices begins with calibration of the temperature-dependent resistance of the sensor against a commercial Ge thermometer. Calibration is carried out using four-probe techniques, with a very small (≈10 nA) ac sensing current chosen to avoid spurious heating. The phonon thermal conductance $G=\dot{Q}/\Delta T$ is obtained by providing a carefully controlled dc heating current (0.2–2 μA) to the source transducer ($\dot{Q}\sim2$–200 nW) while monitoring the resultant small change of temperature in the sensor ($\Delta T\sim5\%\times T$). Almost all of the heat is generated on the hexagonal reservoir while a small portion ($<15\%$, as estimated from geometry) is generated in the beams.

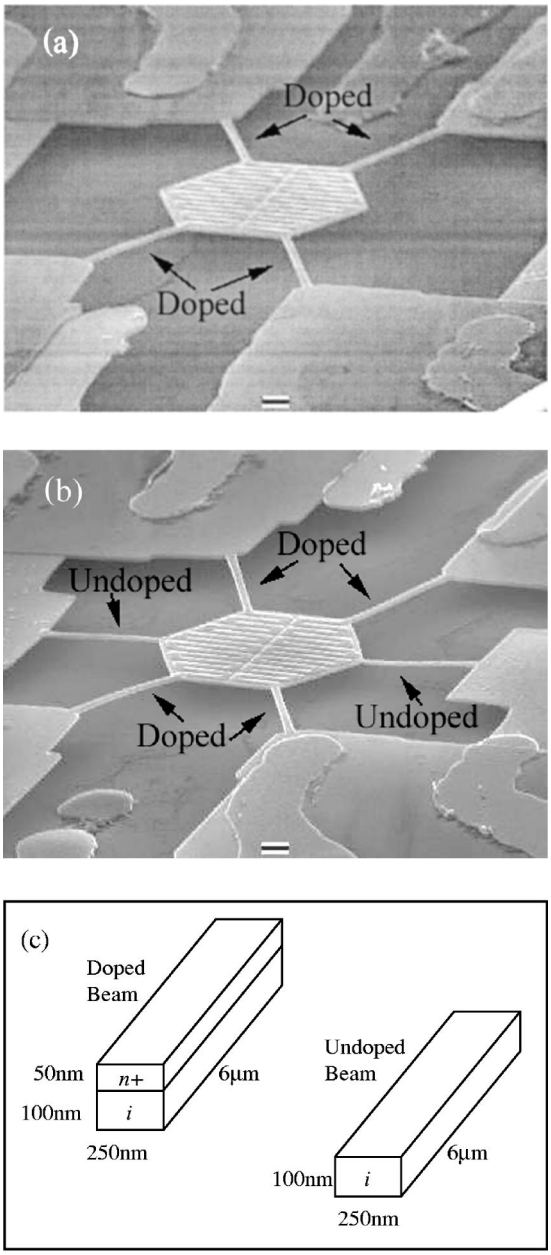

FIG. 1. Scanning tunneling microscopy (SEM) micrographs of typical (a) four-beam and (b) six-beam devices. The captions "Doped" and "Undoped" identify the doped beams and undoped beams that are illustrated in (c).

III. RESULTS: THERMAL CONDUCTANCE OF MESOSCOPIC BEAMS

Our measurements of thermal conductance are performed on three pairs of four- and six-beam devices from 4 to 40 K. The data for one pair are shown in Fig. 2. The others showed quite similar results. We find that the conductance of a six-beam device is significantly higher (50%–100%) than that of a four-beam device. This indicates that the two additional undoped beams of the former provide effective heat transport. In our analysis, we focus on the thermal conductance of an *individual* suspended beam. For a four-beam device *one-quarter* of the total thermal conductance represents the thermal conductance of a single doped beam. To deduce the phonon thermal conductance of a single *undoped beam*, we subtract from the total conductance of the six-beam device the contributions from the four doped beams, as deduced from the four-beam device and divide this by 2. Stated equivalently, the conductance of a single undoped beam is deduced as *one-half of the difference* between the total conductance of the six- and four-beam devices. This subtractive comparison is valid if the two devices are identical except for the two undoped beams. Final inspection of our devices by scanning electron microscopy confirms that differences in dimensions are less than 5%.

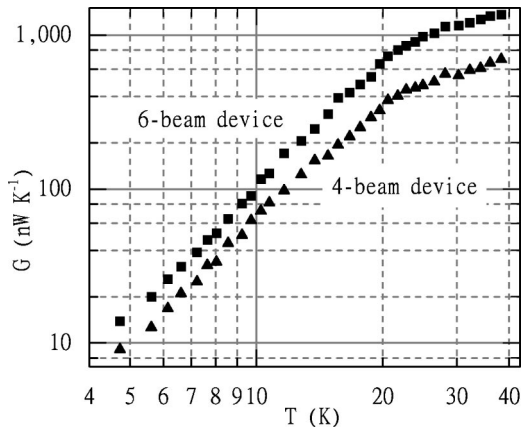

FIG. 2. Thermal conductance G of four- and six-beam devices vs temperature.

We show in Fig. 3 the effective thermal *conductivity* of the beams, which is defined as $g_{\mathrm{eff}}=Gl/A$, where G is the measured thermal *conductance*, l is the length, and A is the cross-sectional area of the beam. The Callaway model, which will be discussed later, generates the curves that fit to the data as shown. It is obvious from the figure that the conductivity of the beams is several orders of magnitudes less than that of macroscopic crystals.[2] We shall discuss this reduced conductivity below in terms of the reduction of the phonon mean free path, arising primarily from (1) the nanoscale transverse sample dimensions and the attendant increased rate of surface scattering of phonons and (2) the increased strength of other scattering mechanisms. The contribution to thermal conduction by electron diffusion in the doped beams is neglected. According to the Wiedemann-Franz law,[10] the thermal conduction by electron diffusion for each beam is $G_{\mathrm{elec}}\approx L_0T/R$, where L_0 is the Lorenz number and $R=6$ kΩ is the electrical resistance of the beam. Thus, the electronic thermal conductance is of order 0.1 nW K^{-1} and is small compared to that by phonons.

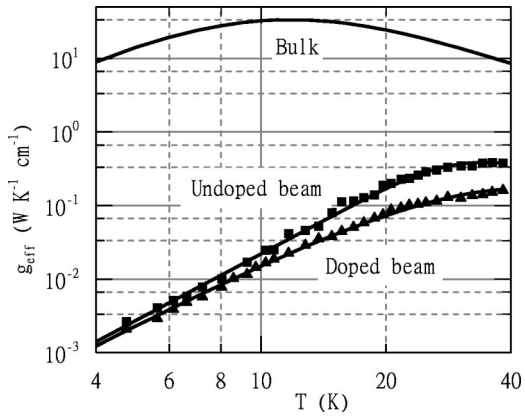

FIG. 3. Comparison between the effective thermal conductivity g_{eff} of doped and undoped beams and that of bulk GaAs. The bulk values are from Ref. 2. The curves are fit by the Callaway model. The fitting parameter values, according to Eq. 2, are $\Lambda_{\mathrm{surf}}=0.65\mu$m and $C=6.5\times10^{-16}$ s K^{-1} for the undoped beam and $\Lambda_{\mathrm{surf}}=0.72$ μm, $A=3.23\times10^{-26}$, $B=2.65\times10^{-40}$ s^3, and $C=6.5\times10^{-16}$ s K^{-1} for the doped beam.

IV. PHONON SCATTERING RATES AND CALLAWAY ANALYSIS

We begin our analysis by deducing phonon scattering rates using the analysis due to Callaway.[2,12] Well below the Debye temperature ($\theta_D=345$ K for GaAs), the thermal conductivity of a bulk crystal is approximated as

$$g=\frac{k_{\mathrm{B}}}{2\pi^2c}\left(\frac{k_{\mathrm{B}}}{h}\right)^3T^3\int_0^{\theta_{\mathrm{D}}/T}\tau(\nu,T)\frac{x^4e^x}{(e^x-1)^2}dx, \qquad (1)$$

where ν is the phonon frequency, $x=h\nu/k_{\mathrm{B}}T$, and c is the phonon group velocity ($c\approx3500$ m/s for GaAs). The total phonon relaxation time $\tau(\nu,T)$ is the inverse of the scattering rate and combines the effect of all scattering mechanisms according to Matthiessen's rule. Note that the applicability of the rule is based on many assumptions including that all scattering mechanisms operate independently:

$$\tau^{-1}=\tau_{\mathrm{surface}}^{-1}+\tau_{\mathrm{electron}}^{-1}+\tau_{\mathrm{defect}}^{-1}+\tau_{\mathrm{phonon}}^{-1} \qquad (2)$$

$$=c_{\mathrm{av}}/\Lambda_{\mathrm{surf}}+A\nu+B\nu^4+C\nu^2Te^{-(\theta_{\mathrm{D}}/aT)}.$$

The surface scattering time is represented as a constant independent of ν and T. The form of the phonon-electron scattering rate is that given by Ziman[13] for a degenerate semiconductor. The point defect scattering rate[17] has a fourth-power dependence on frequency that is common for Rayleigh scattering. Finally, the phonon-phonon scattering time is based on a form widely used in the literature.[14] Here, the exponential term accounts for the fact that the phonon-phonon contribution to the thermal resistance arises solely from high-energy umklapp processes.

For the *undoped beams* the phonon relaxation time contains only the diffuse surface and phonon-phonon scattering terms. For the *doped beams*, given their additional electronic components, phonon-electron and phonon-defect scattering processes are also operative; hence, all four scattering terms are required. The curves fit to the effective thermal conductivity are shown in Fig. 3 along with the experimental result. The fits are quite sensitive to the values of the fitting parameters. In general, a 10% change in a fitting parameter results in a 3%–10% change in the thermal conductivity fit. Moreover, most of the fitting parameters are independent; i.e., the excellence of the fit could not preserved by adjusting two parameters simultaneously. There is an exception between the phonon-phonon and phonon-defect scattering terms that are difficult to differentiate by the fitting alone. However, comparison of the data from the doped and undoped beams allows their separate contribution to be clearly identified.

From the fitting parameters, the separate frequency- and temperature-dependent phonon relaxation time for each mechanism is deduced, according to Eq. (2). The mean free path (MFP) of the phonons is defined as $\Lambda=c\tau(\nu,T)$. At a temperature T, we obtain the average phonon MFP by integrating the frequency dependence of the MFP weighted by the phonon thermal population. Alternatively, a simpler av-

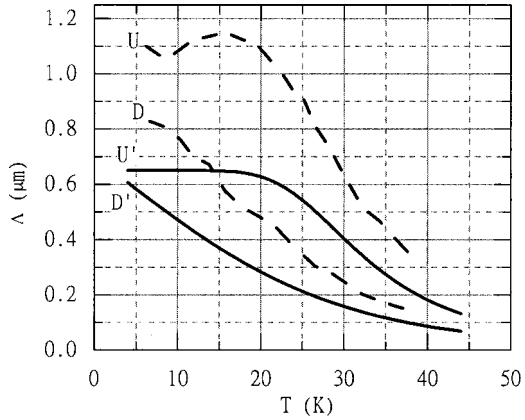

FIG. 4. Mean free path Λ of phonons vs temperature obtained from two different analyses, for undoped and doped beams. Curve U is for undoped beams and D for doped beams, respectively, by the diffusive transport formula. Curve U' is for undoped beams and D' for doped beams by the Callaway model.

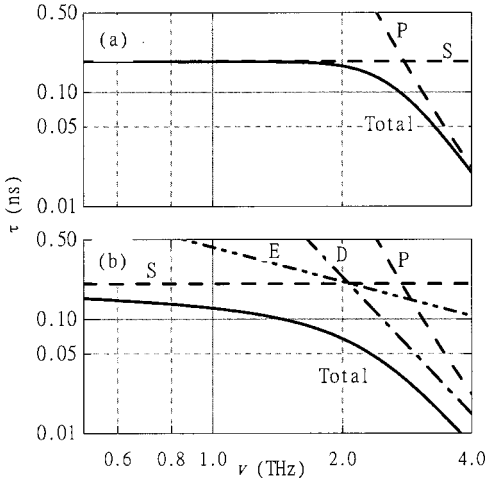

FIG. 5. Phonon relaxation time τ vs phonon frequency as extracted from the Callaway model [Eq. 2] for (a) undoped beams and (b) doped beams. The solid lines depict the total relaxation time. Also shown are relaxation times for other important mechanisms: diffuse surface scattering (curves S), phonon-electron scattering (curve E), phonon-defect scattering (curve D), and phonon-phonon scattering (curves P). For curves P, the temperature is taken to give the average thermal energy of the phonon ($T=h\nu/4k_B$).

erage MFP can be estimated by the diffusive transport formula $g=1/3C_{ph}c\Lambda$, where g is the effective conductivity, C_{ph} is the phonon heat capacity, and c is average phonon group velocity. The results of both analyses are plotted in Fig. 4 for both the undoped and doped beams. The discrepancy between these analyses arises because the Callaway approach emphasizes thermal conduction by high-frequency phonons.

V. DISCUSSION: THERMAL TRANSPORT OF MESOCOPIC BEAMS

Below 20 K, the phonon thermal conductance of the undoped beam displays an approximate T^3 power law. In the framework of the Callaway analysis, this suggests a phonon relaxation time that is independent of frequency and temperature. This constant MFP implied is generally understood to be related to diffuse scattering at the surface and is dependent on the geometry of the sample.[7] We note that the longest phonon MFP estimated from the data (≈ 1.1 μm by the diffusive transport formula) is much shorter than the length of the beams (6 μm). Thus, at the temperature of these experiments, there is minimal possibility for ballistic transport along the length of the beams.

The surface quality of the beams can be estimated from the specularity parameter $p=[(\Lambda/\Lambda_0)-1]/[(\Lambda/\Lambda_0)+1]$.[13] Here, $\Lambda_0=1.12(d_1d_2)^{1/2}$ is the MFP in the limit of completely diffuse surface scattering for a rectangular beam of sides d_1 and d_2. For our beams, Λ_0 is ≈ 0.2 μm. Hence, from the phonon MFP (Λ) obtained at 4 K, p is ≈ 0.7, indicating that phonon surface scattering is only partially specular; i.e., on average, each phonon is specularly reflected only $1/(1-p)\approx 3$ times before being diffusely scattered. This is comparable to the findings of Tighe *et al.* and is somewhat surprising. The topology of the surfaces suggests a roughness only of order 4 nm, which is likely induced by the chemical-assisted ion beam etching (CAIBE) process. By comparison, the thermal phonon wavelength at our lowest temperature exceeds 10 nm. Moreover, polished surfaces of macroscopic crystal used in other experiments[9] have been shown to have a much higher specularity (>0.99). The mechanisms controlling surface specularity in nanostructures clearly warrant further investigation.

At higher temperatures, from 20 to 40 K, the conductivity of both the doped and undoped beams falls far below the values extrapolated from the T^3 power law found below 20 K. According to the Callaway analysis, this must arise from a reduction of the MFP corresponding to an increase in scattering. This phenomenon is very common in bulk crystals beyond 10–15 K when umklapp phonon-phonon processes become dominant. In our mesoscopic beams, however, diffuse surface scattering is so strong that the relative contribution due to phonon-phonon scattering is expected to remain insignificant until much higher temperatures (>40 K). Surprisingly, the phonon-phonon scattering rate [Fig. 5(a)], deduced from the curve fitting of the Callaway analysis, is approximately 10 times higher than corresponding bulk values.

There are two possible reasons that may account for the high scattering rates we have deduced. First, the T^3 power law obtained from the Callaway analysis is based on the Debye phonon density of states (DOS) and a constant phonon group velocity. A realistic dispersion relation of GaAs,[15] however, shows that between 1.5 and 2.5 THz, the phonon DOS is higher than the Debye values. Correspondingly, the phonon group velocity is much smaller than that of the low-frequency phonons. On the other hand, above 3 THz, the actual phonon DOS is much smaller than the Debye values. The reduction of group velocity reduces the phonon ''flow rate'' while the reduction of the DOS reduces the density of thermal energy carriers. Both contribute directly to a lower thermal conduction. Taking the realistic dispersion relation

into account, a simplified model provides a conductivity at 40 K that is only 75% of that obtained from the Debye DOS and constant group velocity. We note that such an argument, while also applicable to bulk crystals, is seldom used. This is because the temperature dependence of the bulk thermal conductivity is dominated by umklapp scattering in the temperature range where this is relevant (>30 K).

The second reason for the high phonon scattering rate deduced may arise from surface scattering of high-frequency phonons. While diffuse surface scattering is generally assumed to be frequency independent in the Callaway analysis, it is quite possible that phonons of higher frequency are scattered more effectively when their wavelengths approach the scale of surface roughness (<4 nm). In this case, the surface specularity parameter for phonons would become further reduced at higher temperatures. If diffuse surface scattering is assumed to be dominant even at 40 K, the average number of specular reflection would decrease to ≈ 1.

The analysis above applies equally well to the doped and undoped beams. However, the data show that from 4 to 40 K the doped beams transport heat less efficiently than the undoped beams. This is evident from both the effective thermal conductivity and MFP's in Figs. 3 and 4. This appears to indicate that dopants in the mesoscopic beams introduce additional, efficient mechanisms for phonon scattering. There are three new components that can be identified: scattering of phonons by mobile electrons,[16] by electrons in donor states,[17] and by point defects.[18] The latter occur due to the mass difference between dopants and host atoms. However, the relaxation rates we deduce from the Callaway analysis [Fig. 5(b)] require an apparent defect density that is ≈ 16 times higher than the known dopant concentration in our heterostructures. Additionally we deduce a phonon-electron scattering rate in our samples that is almost two orders of magnitude higher than that found in macroscopic crystals[2] or obtained from simple models for phonon-electron scattering.[16] The presence of dopants provides extraordinarily strong phonon scattering in nanostructures that requires further investigation.

VI. CONCLUSIONS

We report detailed thermal conductance measurements on suspended GaAs nanostructures and determine the effective thermal conductivity of doped and undoped mesoscopic beams from the data obtained. We determine that from 4 to 40 K diffuse surface scattering plays a major role in phonon transport within nanostructures. The surface specularity of the beams studied appears to be rather low. The presence of dopants is found to have an unexpectedly strong effect on the scattering of phonons. We provide a quantitative estimate of important phonon scattering processes that are operative and find that many of them (surface, defect, and mobile electron scattering) are far more effective in mesoscopic beams than in a bulk crystal.

ACKNOWLEDGMENTS

We gratefully acknowledge support from the NSF under Grant No. DMR-9705411 and from DARPA/MTO/MEMS under Grant No. DABT63-98-1-0012.

[1] M.G. Holland, Phys. Rev. **132**, 2461 (1963).
[2] M.G. Holland, Phys. Rev. **134**, A471 (1964).
[3] R.O. Carlson, G.A. Slack, and S.J. Silverman, J. Appl. Phys. **36**, 505 (1965).
[4] J.W. Vandersande, and C. Wood, Contemp. Phys. **27**, 117 (1986).
[5] C.G. Smith, H. Ahmed, and M.N. Wybourne, J. Vac. Sci. Technol. B **5**, 314 (1987).
[6] A. Potts *et al.*, Semicond. Sci. Technol. **7**, B231 (1992).
[7] T.S. Tighe, J.M. Worlock, and M.L. Roukes, Appl. Phys. Lett. **70**, 2687 (1997).
[8] J.S. Blakemore, J. Appl. Phys. **53**, R123 (1982).
[9] T. Klitsner, J.E. VanCleve, H.E. Fischer, and R.O. Pohl, Phys. Rev. B **38**, 7576 (1998).
[10] A. Potts *et al.*, J. Phys.: Condens. Matter **2**, 1817 (1990).
[11] K. Schwab, E.A. Henriksen, J.M. Worlock, and M.L. Roukes, Nature (London) **404**, 974 (2000).
[12] R. Berman, *Thermal Conduction in Solids* (Oxford University Press, Oxford, 1976), Chap. 4.
[13] J. M. Ziman, *Electrons and Phonons* (Oxford University Press, Oxford, 1960).
[14] See, for example, Y.J. Han, Phys. Rev. B **54**, 8977 (1996) for a discussion of various forms of the phonon-phonon scattering rate.
[15] G. Dolling and R.A. Cowley, Proc. Phys. Soc. London **88**, 463 (1966).
[16] J.M. Ziman, Philos. Mag. **1**, 191 (1956).
[17] R.W. Keyes, Phys. Rev. **122**, 1171 (1961).
[18] P. G. Klemens, in *Solid State Physics, Advances in Research and Applications*, edited by F. Seitz and D. Turnbull (Academic, New York, 1958), Vol. 7.